Powder Technology 258 (2014) 297–303

Contents lists available at ScienceDirect

Powder Technology

journal homepage: www.elsevier.com/locate/powtec

Effective removal of organic dyes by tungstate oxide nanourchins

Liang Xiao, Shishen Zhang, Jianhua Huang *

Department of Chemistry, Zhejiang Sci-Tech University, Hangzhou 310018, People's Republic of China

ARTICLE INFO

Article history:
Received 23 November 2013
Received in revised form 17 February 2014
Accepted 11 March 2014
Available online 19 March 2014

Keywords:
Tungsten oxide
Organic dyes
Adsorption
Intraparticle diffusion

ABSTRACT

$W_{18}O_{49}$ nanourchins were synthesized via a solvothermal reaction of WCl_6 in triethylene glycol. They possessed high specific surface area of 103.4 $m^2.g^{-1}$ and exhibited excellent adsorption capacity for the removal of methylene blue and rhodamine B. The equilibrium adsorption capacity toward methylene blue and rhodamine B reached 150.3 and 81.78 $mg.g^{-1}$, respectively. Oxygen vacancies in $W_{18}O_{49}$ played an important role in the adsorption of organic pollutants. The adsorption kinetics of methylene blue and rhodamine B were both well described by the pseudo-second-order model. The adsorption was found to be controlled by both surface adsorption and intraparticle diffusion. Our product is expected to be a promising material for wastewater treatment.

1. Introduction

Environmental pollution is one of the most important issues in the world today. Every year, a large number of highly toxic and carcinogenic organic dyes are utilized in industries, such as textile, leather, paper, plastics, etc., which will produce plenty of colored wastewater [1–4]. There are several methods to remove the dyes from wastewater, such as membrane separation [5], photocatalytic degradation [6,7], adsorption [8] and biological degradation [9]. Among them, adsorption is considered to be an effective, versatile and economical method for the treatment of pollutants because of its simplicity, high efficiency, insensitivity of toxic materials and low operational costs. What's more, it doesn't bring about any harmful substances [10]. Activated carbon with high specific surface and porous structure has been widely used as an adsorbent for the removal of organic dyes from wastewater [11,12].

Generally, transition metal oxides could be also suitable as adsorbents or catalysts for removal of organic pollutants from water [13]. Many transition metal oxides have been successfully used as adsorbents in wastewater treatment and showed very good ability to remove organic pollutants. For example, Mn_2O_3 exhibited excellent performance of removing phenol in wastewater [14]. NiO [15], manganese oxide [8,16,17], iron oxide [13,18,19], magnetic $CuFe_2O_4$ [20], and MnO-Fe_2O_3 composite [21] were successfully used as adsorbent/catalyst for the removal of azo-dyes. $NiFe_2O_4$ [22] and Fe_2O_3/MgO composite [23] showed good properties on the adsorption of reactive dyes. Manganese oxides [24] and Magnetic manganese oxide [25] were also used as adsorbents for methylene blue (MB) removal from wastewater. Experimental results show that although the specific surface area is a key factor for the adsorption, the adsorption process may depend on various other factors, such as the crystal structure of adsorbent [24], the electrostatic attraction [16] and the hydrogen bonding [25] between adsorbent and adsorbate.

It is noticed that the adsorption properties of the above adsorbents exhibit some limitations, such as acid-nonresistant, or limited adsorption on basic dyes [26]. Tungsten oxide is well-known for its nonstoichiometric properties as the lattice can withstand a considerable amount of oxygen deficiency and has received increasing interest owing to its unique catalytic and adsorption properties. Hexagonal WO_3 nanorods exhibited high adsorption capacity for organic dyes including rhodamine B (RhB) and MB [27]. The results demonstrated that the (001) facet with all coordinatively unsaturated W atoms was favorable for adsorbing RhB. However, monoclinic WO_3 showed very low adsorption capacities for both RhB and MB due to the inactive monoclinic phase [27]. The good adsorption property of WO_3 nanotube bundles with hexagonal phase for MB could be largely attributed to the electrostatic attraction between the tungsten trioxide surface and the MB species [28].

As an important acidic oxide material, $W_{18}O_{49}$ is of special interest due to its unique defect structure and distinct physical and chemical properties [29]. The acidic surface of $W_{18}O_{49}$ nanomaterials enhances their adsorption on basic dyes [26,30,31]. However, the adsorption kinetics and adsorption mechanism of $W_{18}O_{49}$ for organic dyes have not been investigated in these studies. In the present work, $W_{18}O_{49}$ nanourchins were prepared by a template-free solvothermal method. They exhibited excellent adsorption capacity for organic dyes including MB and RhB. The adsorption kinetics and the adsorption mechanism were studied in detail.

---

* Corresponding author. Tel.: +86 571 86843228.
E-mail address: jhhuang@zstu.edu.cn (J. Huang).

http://dx.doi.org/10.1016/j.powtec.2014.03.049

2. Experimental section

2.1. Synthesis

$W_{18}O_{49}$ nanourchins were synthesized via a solvothermal reaction of WCl_6 in triethylene glycol similar with Ref. [29]. Typically, 0.6 g of WCl_6 was added into 30 mL triethylene glycol with constant magnetic stirring for 60 min at room temperature, the solution was then transferred to a 50 mL Teflon-lined autoclave and maintained at 160 °C for 24 h. After cooling naturally down to room temperature, the greenblack precipitates were collected by centrifugation and washed thoroughly with deionized water and ethanol, and then dried at 60 °C for 6 h.

2.2. Characterization

X-ray diffraction (XRD) patterns of the samples were recorded on a DX-2700 diffractometer (Dandong Fangyuan Instrument Co., Ltd., China) using Cu Kα radiation (1.5418 Å). Scanning electron microscope (SEM) images were taken using a Hitachi S-4800 electron microscope. The Brunauer–Emmett–Teller (BET) surface area was measured using nitrogen adsorption–desorption isotherms at 77 K on a Micromeritics ASAP 2020 analyzer. Fourier transform infrared (FT-IR) spectra were collected on a Nicolet Avatar 730 spectrometer using KBr pellets. X-ray photoelectron spectroscopy (XPS) measurements were carried out on a RBD upgraded PHI-5000C ESCA system (PerkinElmer) with Mg Ka radiation ($h\nu = 1253.6$ eV). Ultraviolet–visible–near infrared (UV–vis–NIR) absorption spectra were recorded with a Perkin Elmer Lambda 950 with integrating sphere.

2.3. Organic dye adsorption

The adsorption of MB and RhB on $W_{18}O_{49}$ and its calcined products was studied at 25 °C. It was performed as follows: A series of 0.1 L conical flasks containing 0.05 L MB aqueous solution with a concentration of 200 $mg.L^{-1}$ or RhB aqueous solution with a concentration of 80 $mg.L^{-1}$ were first prepared, and 0.05 g adsorbent was added into every conical flask. They were then sealed, moved to a thermostated shaker (Jintan Jinnan Instrument Manufacturing Co., Ltd.) and kept under a shaking speed of 150 rpm at natural pH (the pH value of MB and RhB aqueous solutions were 6.89 and 4.00, respectively). The conical flask was taken from the shaker at various adsorption intervals, and the adsorbent was separated by centrifugation. The concentrations of MB and RhB left in the supernatant solution at various adsorption intervals were monitored by a UV-2480H spectrometer (Unic, (Shanghai) Instrument Co., Ltd., China) and determined by measuring absorbance changes at their respective absorption maxima, 664 and 554 nm. In the experiments, each datum was obtained from an individual conical flask and therefore no correction was necessary due to withdrawal of sampling volumes.

3. Results and discussion

3.1. Characterization of adsorbents

The XRD pattern of the solvothermal product is shown in Fig. 1(a). All peaks in this pattern can be well indexed to a monoclinic $W_{18}O_{49}$ phase (cell constants: $a = 18.28$ Å, $b = 3.775$ Å, and $c = 13.98$ Å; JCPDS card: 05-0392). The narrow peak at 23.5° indicates that $W_{18}O_{49}$ is elongated along the (010) plane [29]. After calcination at 300 °C (referred as $W_{18}O_{49}$-300 hereafter), a similar XRD pattern is observed (Fig. 1(b)), however, the peak intensities decrease, implying that oxidation may takes place on the surface and the oxygen vacancies in the surface disappear after calcination at 300 °C [29]. When the calcination temperature increases to 400 °C, pure monoclinic WO_3 phase (cell constants: $a = 7.297$ Å, $b = 7.539$ Å, and $c = 7.688$ Å; JCPDS card: 43-1035) is obtained, see Fig. 1(c).

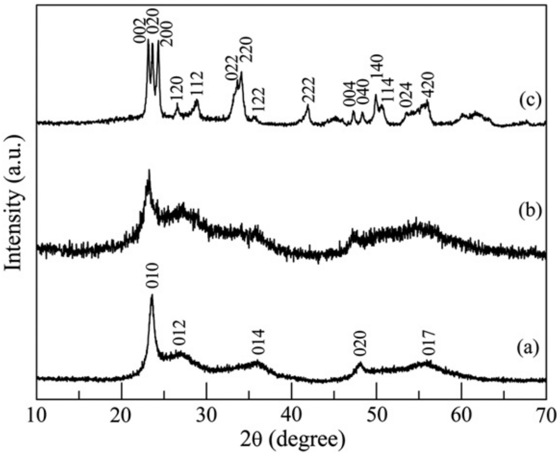

Fig. 1. XRD patterns of (a) solvothermal sample and its calcined sample at (b) 300 and (c) 400 °C.

The morphology of samples was studied through SEM observation. Fig. 2(a) shows that $W_{18}O_{49}$ possesses an urchin-like structure consisting of nanowires with a diameter about 30 nm. Similar morphology is observed for $W_{18}O_{49}$-300 (Fig. 2(b)). Fig. 2(c) shows that nanowires transform into nanoparticles with a size of 50–100 nm in WO_3. From Fig. 2, we obviously observe the color change from the initial greenblack to cyan and to yellow after calcination at 300 and 400 °C, respectively.

We have measured the specific surface area of the samples using the multipoint Brunauer–Emmett–Teller (BET) method. $W_{18}O_{49}$ and $W_{18}O_{49}$-300 exhibit type IV isotherms with a small hysteresis loop in the relative pressure range of 0.4–1.0, and they have similar pore size distribution (data not shown). The calculated BET specific surface areas (S_{BET}) are 103.44 and 104.45 $m^2.g^{-1}$ for $W_{18}O_{49}$ and $W_{18}O_{49}$-300, respectively. While it decreases to 33.41 $m^2.g^{-1}$ for WO_3. The small S_{BET} of WO_3 could be attributed to the crystal growth after calcination at 400 °C.

3.2. Adsorption isotherms

Inspired by the high specific surface area, we believe $W_{18}O_{49}$ would be quite effective to remove organic pollutants in water. MB, a common cationic dye in the textile industry, was chosen as a typically weakly biodegradable organic pollutant. Fig. 3(a) shows the UV–vis absorption spectra of MB solutions before and after addition of $W_{18}O_{49}$. The MB solution was diluted for 25 times before UV–vis measurement. The characteristic absorption of MB at 664 nm was chosen as the indicator to be monitored during the adsorption process. It shows that the adsorption is quite rapid initially and 44% of MB is removed in the first 20 min, then it gradually slows down and ultimately reaches the adsorption equilibrium. Under the same experimental condition, the MB removal capacities of $W_{18}O_{49}$-300 and WO_3 were also examined. Fig. 3(b) shows the adsorption capacity of $W_{18}O_{49}$, $W_{18}O_{49}$-300 and WO_3 for MB removal as a function of adsorption time. The adsorption capacity at time t, q_t ($mg.g^{-1}$), is calculated by the equation $q_t = (C_0 - C_t) \cdot V/m$, here V (L) is the volume of solution, and m (g) is the mass of adsorbent. C_0 and C_t are the concentration of MB solution before adsorption and at various adsorption intervals, respectively. The equilibrium adsorption capacity of $W_{18}O_{49}$ is 150.3 $mg.g^{-1}$, higher than that of reported transition metal oxides, such as manganese oxide [24,25], WO_3 [27,28], tungsten oxide hollow urchins [31], as shown in Table 1. It is a little smaller than that of $W_{18}O_{49}$ nanowire networks reported very recently [26] probably due to the smaller S_{BET} of our sample. The result suggests that the as-prepared $W_{18}O_{49}$ has good potential as an efficient adsorbent for organic wastewater treatment. However, the maximum adsorption capacity of $W_{18}O_{49}$-300 decreases to 77.2 $mg.g^{-1}$. And it is only 14.7 $mg.g^{-1}$ for WO_3 similar with the previous reports [27,31].